U.S.NRC
United States Nuclear Regulatory Commission
Protecting People and the Environment

RIL 2021-06

Assessing Site Amplification Variability Using Downhole and Rock-Soil Pairs Site Recordings

Date Published: August 2021

Prepared by:

V. Graizer[1]
D. Seber[2]
Scott Stovall[1]

U.S. Nuclear Regulatory Commission

[1] NRC Seismologist
[2] NRC Branch Chief

Research Information Letter
Office of Nuclear Regulatory Research

Disclaimer

This report does not contain or imply legally binding requirements. Nor does this report establish or modify any regulatory guidance or positions of the U.S. Nuclear Regulatory Commission. This report is not binding on the Commission.

Page intentionally left blank

EXECUTIVE SUMMARY

For nuclear power plants licensed after January 10, 1997, Title 10 of the *Code of Federal Regulations* (10 CFR) Part 50, “Domestic licensing of production and utilization facilities,” and 10 CFR 100.23, “Geologic and seismic siting criteria,” establish the seismic design basis. Appendix S, “Earthquake Engineering Criteria for Nuclear Power Plants,” to 10 CFR Part 50 defines the safe-shutdown earthquake: “Safe-shutdown earthquake ground motion is the vibratory ground motion for which certain structures, systems, and components must be designed to remain functional.” The regulation in 10 CFR 100.23 requires that the applicant determine the safe-shutdown earthquake and its uncertainty. A probabilistic seismic hazard assessment (PSHA) is an acceptable method to capture uncertainty.

Traditionally, ground motion models and PSHAs are developed based on an ergodic assumption, with a broad range of uncertainties. An ergodic process is a random process in which the distribution of a random variable in space is the same as the distribution of that same random variable at a single point when sampled as a function of time (Anderson and Brune, 1999). An ergodic assumption is made when a PSHA treats that spatial uncertainty of ground motions as an uncertainty over time at a single point. This usually results in overly conservative values in hazard calculations. Recently, the practice has trended towards nonergodic PSHAs, when additional information about the site of interest is available. It has been previously shown that, with a sufficient number of earthquake recordings, the mean site amplification functions (SAFs) can be well determined, but individual event ratios can be quite variable. From this point of view, it is important to assess and quantify observed variabilities in SAFs obtained from earthquake recordings.

This report assesses site-specific variability in empirical SAFs calculated using earthquake recordings with a total of 13 datasets, including data from the six California strong motion downhole arrays at Treasure Island, Turkey Flat, San Francisco Bay Bridge, Crockett Carquinez Bridge, Corona Bridge, and Garner Valley and also three soil-rock pair stations. The two- and three-dimensional effects, which include out-of-plane reflection/refraction, focusing, scattering, and conversion of wave types, produce significant variability in empirical SAFs from earthquake data recorded at a single station. This analysis demonstrates that log-natural standard error $\sigma_{ln(f)}$ (sigma) in empirical SAFs calculated using downhole array data can be approximated by a linear function with an average value of 0.221 (1.25 times) in the frequency range of data processing. By using a constant in the frequency range of 0.1–10 hertz, $\sigma_{ln(f)}$ can be well approximated and is slightly increasing at higher frequencies for rock-soil pairs. Because of spatial variability, the rock-soil pairs sigma is higher than that of downhole arrays with an average of 0.272 (1.31 times). Variability in empirical SAFs helps constrain single-station, nonergodic sigma estimates.

Keywords: Arrays Seismic Motion, Rock and Soil Motions, Site Amplification Variability

INTRODUCTION

For nuclear power plants licensed after January 10, 1997, Title 10 of the *Code of Federal Regulations* (10 CFR) Part 50, “Domestic licensing of production and utilization facilities,” and 10 CFR 100.23, “Geologic and seismic siting criteria,” establish the seismic design basis. Appendix S, “Earthquake Engineering Criteria for Nuclear Power Plants,” to 10 CFR Part 50 defines the safe-shutdown earthquake: “Safe-shutdown earthquake ground motion is the vibratory ground motion for which certain structures, systems, and components must be designed to remain functional.” The regulation in 10 CFR 100.23 requires that the applicant determine the safe-shutdown earthquake and its uncertainty. A probabilistic seismic hazard assessment (PSHA) is an acceptable method to capture uncertainty.

Traditionally, ground motion models and PSHAs are developed based on an ergodic assumption, with a broad range of uncertainties. An ergodic process is a random process in which the distribution of a random variable in space is the same as the distribution of that same random variable at a single point when sampled as a function of time (Anderson and Brune, 1999). An ergodic assumption is made when a PSHA treats that spatial uncertainty of ground motions as an uncertainty over time at a single point. This usually results in overly conservative values in hazard calculations. Recently, the practice has trended towards nonergodic PSHAs, when additional information about the site of interest is available. It has been previously shown that, with a sufficient number of earthquake recordings, the mean site amplification functions (SAFs) can be well determined, but individual event ratios can be quite variable (e.g., Field et al., 1992; Boore, 2004). From this point of view, it is important to assess and quantify observed variabilities in SAFs obtained from earthquake recordings.

This report assesses site-specific variability in empirical SAFs observed using recorded earthquake data from the six California strong motion downhole arrays at Treasure Island, Turkey Flat, San Francisco Bay Bridge, Crockett Carquinez Bridge, Corona Bridge, and Garner Valley and also three rock-soil pairs of stations. These downhole arrays have at least one sensor in rock site condition. It also considers 13 alternative scenarios, giving the most attention to the data from the Treasure Island and Turkey Flat arrays because these sites have been studied extensively and have detailed geological and geotechnical information. Presented uncertainties in SAFs are caused by randomness of earthquake locations and magnitudes and can be considered to be aleatory.

ANALYSIS OF THE TREASURE ISLAND DOWNHOLE ARRAY RECORDS

Treasure Island (TI) is an artificial island in San Francisco Bay in California. Constructed in the 1930s for the 1939 Golden Gate International Exposition (Figure 1, left panel), the island was created by fine-to-medium-grained sand dragged from San Francisco Bay and used as a fill material. The fill material was deposited hydraulically by a clamshell dredge. Below the fill and native sand is a layer of bay mud composed of silty clay with regions of sand and silt. The older bay sediments of Pleistocene age are generally stiff to sandy, silty, or peaty clays that extend down to Franciscan bedrock (Figure 1, right panel) (de Alba et al., 1994).

This report analyzes high-quality, low-amplitude earthquake data recorded at TI and Yerba Buena Island (YBI) near San Francisco, CA. Most publications describe the YBI geology as rock (e.g., Darragh and Shakal, 1991). TI is a manmade island situated between San Francisco and

Oakland, CA, and attached to the natural YBI by a short causeway (Figure 1, left panel). Many places on TI experienced liquefaction during the moment magnitude (**M**) 6.9 Loma Prieta earthquake of 1989 (Ferritto, 1992). Following this earthquake, the California Geological Survey (CGS), with support from the National Science Foundation, installed the TI array in 1992 to study the response of a soft soil over rock geologic structure to earthquake motion (Darragh et al., 1993; de Alba et al., 1994; Graizer, 2014). The TI downhole array had sensors located in the bedrock (104- and 122-meter (m) depths), alluvium (31- and 44-m depths), and artificial fill (7- and 16-m depths) and at the surface (shown with triangles in Figure 1, right panel). The downhole instrument at 122-m depth was added in 1996. In September 2003, the original digital 12- and 16-bit instrumentation was replaced with modern 19-bit instruments (Graizer and Shakal, 2004).

Figure 1 (right panel) shows the velocity and geology profiles at the TI array. Weathered Franciscan shale and sandstone are encountered at 88 m beneath the site, with more competent sandstone found at a depth of about 98 m (Darragh and Idriss, 1997). The U.S. Geological Survey performed original downhole *S*-wave velocity measurements in the 104-m deep hole (Gibbs et al., 1992). More recent *S*-wave velocity averaging was performed based on the *P*-*S* suspension logging measurements conducted in the deepest 122-m borehole drilled in 1996 (Graizer and Shakal, 2004). *S*-wave velocities vary from ~134 meters per second (m/s) in the gray fine sand layer to ~2,523 m/s in the deepest Franciscan bedrock (Figure 1, right panel).

The authors downloaded 26 processed earthquake records from the Center for Engineering Strong Motion Data (CESMD) https://strongmotioncenter.org/) recorded by the CGS Station Treasure Island—Geotechnical Array. All recordings are low-amplitude ground motions with maximum peak ground acceleration (PGA) at the surface of 0.038 g (Table 1). In contrast to previous studies of TI recordings (Graizer, 2014), all except the local magnitude M_L 5.0 1999 Bolinas earthquake were recorded by the array after September 2003 with the newly installed modern 19-bit instruments that replaced the original 12- and 16-bit instrumentation (Graizer and Shakal, 2004). Most of the older records were not used in order to avoid problems with low signal-to-noise ratios especially affecting bedrock downhole recordings because of the lower resolution of older equipment. First, the authors studied amplification of ground motions from the deepest sensor in Franciscan bedrock at the depth of 122 m to the surface (Figure 1, right panel) by comparing 5-percent damped response spectral accelerations of earthquake recordings. At the second stage, the analysis examined amplification from bedrock recordings at a depth of 104 m to the surface.

Figures 2 and 3 demonstrate examples of recorded accelerations and calculated displacements at different depths representing the two different types of recordings: (1) relatively simple signals dominated by *S*-waves (Figure 2) and (2) signals dominated by surface waves (Figure 3).

Figure 4 demonstrates response spectral ratios of motions at the surface relative to the bedrock at 122-m depth. As is typical in earthquake engineering practice, individual earthquake SAFs at each frequency are calculated as a ratio of geometric means of the two horizontal components oriented at 90 and 360 degrees:

$$SAF_{downhole} = \frac{Geomean(A^{TI}_{surf,360},\ A^{TI}_{surf,90})}{Geomean(A^{TI}_{122m,360},\ A^{TI}_{122m,90})} \quad (1)$$

The main peak in the response spectral site amplification is observed at ~0.8 hertz (Hz), and the second peak is at ~1.75 Hz (Figure 4). As shown by Haskell (1960), for a vertically incident *SH*-wave on a plane layer having a shear wave velocity V_S and a thickness *h,* mechanical resonances occur at frequencies f_n (quarter wavelength approximation):

$$f_n=(2n+1)\times V_S/4h \quad (2)$$

The lowest frequency (first mode) can be associated with the alluvium-bedrock interface at the 88-m depth characterized by the *S*-wave velocity increase from 386 to 1,230 m/s (Figure 1, right panel). Using average *S*-wave velocity of V_S ~267 m/s in the upper layer of thickness *h* = 88 m results in the resonance frequency of 0.76 Hz, which is close to the average empirical value of 0.8 Hz. The second peak in SAF at 1.75 Hz can be associated with the bay mud-alluvium interface at the depth of 28.8 m, characterized by a significant *S*-wave velocity increase from 176 to 317 m/s.

SAFs shown in Figure 4 (upper panel) demonstrate significant variations in amplitudes of the first peak at ~0.8 Hz from a factor of ~4 to ~13 for individual events. These SAFs can be split into the two different groups depending on the amplitudes of the first ~0.8-Hz peak: the lower amplification group (LAG) events (maximum peak averages ~4.9) (Figure 4, middle panel) and the higher amplification group (HAG) events (maximum peak averages ~9.0) (Figure 4, lower panel). The first group (LAG) includes 14 events, and the second one (HAG) includes 12 events (Table 1). Events that produce lower amplitude spectral ratios are mostly close-by earthquakes with dominant direct *S*-waves and relatively low-amplitude surface waves (Figure 2). Earthquakes producing relatively higher amplitude response spectral ratios are more distant earthquakes with larger amplitude surface waves compared to *S*-wave amplitudes (Figure 3).

Figure 5 demonstrates mean ±1 standard deviation response SAFs for all 26 surface/122-m depth records and also for the LAG and HAG. As expected, the group that includes all events demonstrates higher log-natural sigma $\sigma_{ln}(f)$ than that of the low SAF events. In all cases, average sigmas are almost flat with only slight change at frequencies higher than 30 Hz.

At the second stage, the authors calculated SAFs for 11 surface/104-m depth available records. Unfortunately, after 2007, the three channels in the 104-m deep downhole died and did not record earthquakes. SAFs shown in Figure 6 demonstrate first and second peaks at the same frequencies of 0.8 and 1.8 Hz and also significant variations in amplitudes of the first peak in individual events. This group of recordings demonstrates practically flat log-natural sigma $\sigma_{ln}(f)$, very similar to that of 122-m downhole up to the frequency of 30 Hz. In the frequency range of data processing of 0.3–40 Hz, average sigma is slightly higher for the surface/104-m case (0.202 versus 0.189).

TREASURE ISLAND AND YERBA BUENA ISLANDS GROUND MOTIONS

In the next series of tests, the analysis compares YBI surface recordings at two nearby stations with the response of the TI array surface data (downhole horizontal Channels 1 and 3 of CGS Station 58642). The stations are (1) YBI CGS Station 58163 and (2) YBI CYB USGS-NCSN station (Table 2).

TI is connected by a small isthmus to YBI with the distance between those sites of 2.20 and 2.25 kilometers (km) (Figure 7). Most publications describe the geology of YBI as rock (Franciscan formation with a mix of sandstone, limestone metamorphic, and other rocks) (Darragh and Shakal, 1991; Darragh and Idriss, 1997; Baise et al., 2003), while the CESMD Web site (https://strongmotioncenter.org/) estimates V_{S30} at 660 m/s and considers it to be Class C. Liquefaction occurred at TI during the 1989 **M** 6.9 Loma Prieta earthquake (Ferritto, 1992; de Alba et al., 1994).

The authors downloaded YBI data from the CESMD for seven earthquakes that were also recorded by the TI array surface channels. Figure 8 (upper panel) demonstrates horizontal component response spectral ratios between the TI surface and YBI. The data were split into two groups: five records from earthquakes with **M**≤4.5 and all seven events including the **M** 6.9 Loma Prieta and the South Napa **M** 6.0 earthquakes. Because of liquefaction at TI, the Loma Prieta record is affected by the nonlinearity with a shift of peak SAF toward low frequencies. As expected, $\sigma_{ln(f)}$ is lower for the first group of smaller events not affected by nonlinearity. The two main peaks in site amplifications are at the frequencies of ~0.8 and 1.8 Hz, demonstrating similarity to those of the TI downhole array shown in Figures 4 through 6.

A number of previous studies (e.g., Darragh and Shakal, 1991) have used rock ground motions at YBI as a reference site to estimate the site response at TI applying a one-dimensional equivalent linear approach. Baise et al. (2003) demonstrated that a two-dimensional basin structure is needed to analyze TI site response. A comparison of SAFs from the YBI and TI bedrock 122-m depth recordings in Figure 8 (lower panel) demonstrates an average amplification of 3.5 times at 10–20 Hz at the YBI relative to TI bedrock, while at frequencies higher than 30 Hz, the difference is about 2.35 (close to the theoretical one of ~2.0) between the media motion relative to the outcrop. These comparisons show that the YBI site is not an ideal rock site input for the TI surface recordings.

TURKEY FLAT ARRAY RECORDINGS

The CGS established the Turkey Flat Site Effects International Test Area in 1987, in a shallow valley at Turkey Flat, located 8 km southeast of the town of Parkfield and about 5 km east of the San Andreas Fault in central California. The array was intended to provide data with which to investigate the accuracy and consistency of current methods for estimating the effects of site conditions on ground surface motions (Real and Tucker, 1988). Figure 9 shows the location of the Turkey Flat strong motion array and epicenters of the eight earthquakes used in the prediction exercise provided by the CGS and two additional events (9 and 10), shown in Table 3, downloaded from the CESMD at https://strongmotioncenter.org/.

The Turkey Flat array is located in a northwest-trending valley within the central California Coastal Range. The valley is filled with a relatively thin layer of stiff alluvial sediments with basement rock outcrops at the south and north ends of the valley (Figure 10, left panel). The valley is about 6.5 km long and 1.6 km wide and is aligned with the southwest plunging Parkfield syncline (Real and Tucker, 1988). Turkey Flat was chosen as a test area to begin with a geologically simple site where a moderate event producing strong motion is expected before moving to more complicated sites.

The Turkey Flat array includes four recording sites: Rock South or Turkey Flat #1 (TF#1) (R1 in Figure 10), Valley Center or Turkey Flat #2 (TF#2) (V1), Valley North or Turkey Flat #3 (TF#3)

(V2), and Rock North or Turkey Flat #4 (TF#4) (R2). Surface instruments were installed at each of these sites, and downhole instruments were installed at the Rock South (R1) and Valley Center (V1) sites. Downhole instrument D1 was located at a depth of approximately 24 m at the Rock South site, and downhole instruments D2 and D3 were located at depths of 10 m and 23.5 m, respectively, at the Valley Center. Valley Center instrument D3 (23.5-m depth) was located about 1 m below the soil/rock boundary. Each instrument location included a three-component force-balance accelerometer and a velocity transducer with 12-bit solid-state digital recording. Unfortunately, the downhole E-W oriented sensor at TF#1 did not work. For reference, the distance from V1 to V2 is about 510 m, from V1 to R1 about 850 m, and from V2 to R2 550 m. The distance between R1 and R2 is about 1,600 m (Figure 10, left panel).

In 1987–1988, multiple investigation teams, both domestic and abroad, carried out a comprehensive program of site characterization. The teams conducted a broad range of field and laboratory geophysical and geotechnical tests. Eight boreholes were drilled through valley sediments into the underlying basement rocks, in which in situ testing was performed and rock and sediment samples were acquired for laboratory analysis. Shear-wave velocity (Figure 10, right panel) was measured in boreholes at the two vertical arrays using downhole, crosshole, and suspension logging methods performed by numerous groups, including LeRoy Crandall and Associates, Hardin Lawson Associates, QEST Consultants, OYO Corporation, Kajima Corporation, the California Division of Mines and Geology (renamed California Geological Survey in 2006), and Woodward–Clyde Consultants (Real et al., 2008; Haddadi et al., 2008; Real and Tucker, 1988).

All records used for this analysis except for the **M** 6.0 Parkfield 2004 earthquake are low-amplitude ground motions indicative of mostly linear site amplifications (Table 3). The Parkfield earthquake was recorded at an epicentral distance of less than 10 km with PGA up to 0.3 g at the TF#2 (Valley Center) site. Usually, amplitudes higher than 0.2–0.3 g are considered to be the level where nonlinearity effects start. According to the results compiled by Kramer (2009), the site responded essentially linearly in the 2004 Parkfield event.

One of the purposes of establishing the Turkey Flat array and an international test area was to perform a blind test experiment similar to that done in typical construction projects. In the first phase of the blind test experiment, participants were provided with all available subsurface data and the recorded R1 rock motions and asked to predict the response of the Valley Center V1 soil motion 850 m apart. In the second phase, which did not begin until all first-phase predictions had been received, participants were provided with the D3 motions and asked to predict the D2 and V1 motions. A number of papers describe the results of the experiment (e.g., Kwok et al., 2008; Kramer, 2009).

All the strong motion earthquake records except for Parkfield main shock were processed in the frequency range of 0.3–40 Hz. The **M** 6.0 Parkfield record was processed in the frequency range of 0.125–40 Hz.

This report considers empirical SAFs. Site amplifications were calculated for the following four cases:

(1) Valley Center downhole TF#2 bedrock (23.5-m depth) to surface (Figure 11)
(2) Rock South (TF#1) to Valley Center (TF#2) surface motions (Figure 12)

(3) Rock North (TF#4) to Valley North (TF#3) (Figure 13)
(4) Combined rock (Rock South + Rock North) to combined soil (Valley Center + Valley North) (Figure 14)

Empirical SAFs demonstrate significant variabilities for different events (Figures 11 through 14), with the average log-natural sigma varying in the range from σ_{ln}=0.262 to σ_{ln}=0.340 with the highest variability observed in the Rock South–Valley Center outcrops (Figure 12), and the lowest for Rock North–Valley North outcrops (Table 4 and Figure 13).

The transfer function V1 (TF#2 surface) – R1 (TF#1 surface) has the highest natural variability of σ_{ln}=0.340 between analyzed pairs. Natural variability in SAFs between TF#2 downhole bedrock (23.5 m deep) and surface motion is relatively high (σ_{ln}=0.288), considering the relatively simple Turkey Flat geologic structure. Tsai et al. (2017) suggested that the two-dimensional effect influenced the response at sites located near the edge of the basin and makes SAFs dependent on wave propagation paths.

ADDITIONAL DOWNHOLE DATA AND SUMMARY RESULTS

This study also included two sets of 16 earthquakes recorded at the Garner Valley downhole array (GVDA) at the surface and at the depths of 50 m (V_S=580 m/s) and 150 m (V_S=3,000 m/s). GVDA records were downloaded from http://nees.ucsb.edu/data-portal. Appendix A (Figure A-1) shows the GVDA sensor locations and *P*- and *S*-wave velocity profiles. GVDA σ_{ln} demonstrates the same behavior as others outlined above: it is almost flat from 0.3 to 40 Hz (Figure 15).

Additionally, the authors analyzed earthquake recordings from the three CGS instrumented strong-motion downhole arrays: San Francisco Bay Bridge with the deepest sensor at 39.9 m and corresponding V_S ~2,000 m/s (10 earthquakes), Crockett Carquinez Bridge #2 with the deepest sensor at 125 m and V_S >1,000 m/s (8 earthquakes), and Corona–I15/Hwy 91 (11 earthquakes) with the deepest sensor at 41.8 m and V_S ~2,000–3,000 m/s. Data were downloaded from the CESMD at https://strongmotioncenter.org/. Appendix A (Figures A-2, A-3, and A-4) shows schematics of downhole locations and *P*- and *S*-wave velocity profiles.

Figure 15 and Table 4 show a compilation of all data from downhole arrays and an average sigma. In almost all cases, log-natural sigma can be approximated by linear dependence with a low slope. Average logarithmic sigma is practically flat in the frequency range 0.1 to 100 Hz.

All this can be considered as aleatory variability and also as the lowest end of nonergodic site-specific sigma. In average log-natural sigma, $\sigma_{ln}(f)$ from downhole array data varies:

$$\sigma_{ln}(f) = 0.0000005 \times f + 0.2351 \quad (3)$$

In the data processing frequency range of 0.3–40 Hz, standard error $\sigma_{ln}(f)$ in empirical site amplification has an average value of 0.221 (1.247 times the mean value of SAF).

This variability in site amplification is due to variations in site-to-source azimuths, wave propagation paths and wave types, magnitudes of earthquakes, and nonlinearity effects modifying amplitudes of ground motions at the site. All data considered in this paper except for

the moment magnitude M_W 6.9 Loma Prieta 1989 and the M_W 6.0 Parkfield 2004 earthquakes are low-amplitude recordings with no nonlinearity effects.

For soil-rock pairs, the average sigma $\sigma_{ln}(f)$ can be approximated as follows:

$$\sigma_{ln}(f) = 0.0017 \times f + 0.2525 \quad (4)$$

As expected, because of spatial variability the soil-rock pair sigma is higher than that of the downhole arrays with an average of 0.272 (1.31 times the mean value of SAF) in the 0.3–40 Hz frequency range (Figure 16). The increase of sigma at high frequencies can be explained by (1) increased randomness at frequencies ≥10 Hz, (2) variation of incident wave angles, (3) variations in media resulting from different paths, and (4) increase of instrumental noise at higher frequencies.

The results of this study agree with Boore's (2004) observation that variability in ground motions is large, making it difficult to accurately predict site- and earthquake-specific response, and with its recommendation to concentrate on predicting mean amplifications for many events.

CONCLUSIONS

This analysis assessed site-specific variability in empirical SAFs calculated using earthquake recordings of a total of 13 datasets, including data from the six California strong motion downhole arrays at Treasure Island, Turkey Flat, San Francisco Bay Bridge, Crockett Carquinez Bridge, Corona Bridge, and Garner Valley and also three soil-rock pairs of stations.

In the frequency range of 0.1–100 Hz, log-natural standard error $\sigma_{ln}(f)$ in empirical downhole site amplification can be approximated by a linear function with an average value of 0.221 (1.25 times the mean value of SAF). For frequencies ≤10 Hz $\sigma_{ln}(f)$, function is practically flat and starts increasing at higher frequencies for soil-rock pairs. The lowest sigma corresponds to the downhole amplification associated with the vertically propagating *S*-waves, while the highest sigma is associated with a rock-soil TF#1 and TF#2 pair where rock station is located near the edge of the two-dimensional basin. As expected, because of spatial variability in soil, the rock pairs sigmas on average are higher (0.272) than those of downhole arrays (average of 0.221) (Figure 16).

The two- and three-dimensional effects, which include lateral refraction, focusing, scattering, and conversion of wave types, produce significant variability in empirical SAFs from earthquake data recorded at a single station and help constrain single-station, nonergodic sigma estimates. The results also give insights into the accuracy that can be achieved in site response predictions. Standard error estimates based on downhole array data represent aleatory variability and can also be considered as the lowest end of nonergodic site-specific sigma.

DATA AND RESOURCES

GVDA data and information were downloaded from http://nees.ucsb.edu/data-portal. All other earthquake records and downhole information were downloaded from the CESMD at https://strongmotioncenter.org/.

ACKNOWLEDGMENTS

We appreciate help from Hamid Haddadi and David Branum in providing additional strong motion data and supporting information about California Geological Survey stations. We thank J.P. Stewart for sharing Turkey Flat geotechnical profiles data.

REFERENCES

Anderson, J., and J. Brune (1999). “Probabilistic seismic hazard assessment without the ergodic assumption,” *Seism. Res. Lett.* **70,** 19–28.

Baise L.G, S.D. Glaser, and D. Dreger (2003). “Site response at Treasure and Yerba Buena Islands, California,” *Journ. Geotechnical and Geoenvironmental Engineering*. **129** (5):415–426.

Boore, D.M. (2004). “Can site response be predicted?” *Journ. Earthquake Engineering*. **8**, Special Issue 1. 1–41.

Darragh, R.B., and I.M. Idriss (1997). “A Tale of Two Sites: Gilroy #2 and Treasure Island Site Response Using an Equivalent Linear Technique,” Earthquake Engineering Research Institute, Oakland, CA.

Darragh, R.B., and A.F. Shakal (1991). ‘‘The site response of two rock and soil station pairs to strong and weak ground motion,’’ *Bull. Seismol. Soc. Am.,* **81**, 1885–1899. Darragh, R., M. Huang and A. Shakal (1993). "Processed CSMIP strong-motion data from the Treasure Island geotechnical array from the Gilroy area earthquake of January 16, 1993." *Calif. Div. Mines and Geology, OSMS 93-09,* 37 p.

de Alba, P., J. Benoit, D.G. Pass, J.L. Carter, T.L. Youd, and A.F. Shakal (1994). “Deep instrumentation array at Treasure Island Naval Station,” *U.S. Geol. Surv. Prof. Pap. 1551-A,* 155–168.

Ferritto, J.M. (1992). “Ground motion amplification and seismic liquefaction: A study of Treasure Island and the Loma Prieta earthquake,” *Naval Civil Engineering Laboratory (NCEL) Technical Note* 92-21874, Port Hueneme, CA.

Field, E.H., K.H. Jacob, and S.E. Hough (1992). “Earthquake site response estimation: A weak-motion case study,” *Bull. Seism. Soc. Am.* **82**, 2283–2307.

Gibbs, J.F., T.E. Fumal, D.M. Boore, and W.B. Joyner (1992). “Seismic velocities and geological logs from borehole measurements at seven strong-motion stations that recorded the Loma Prieta earthquake,” U.S. Geological Survey Open-File Report 92-287, Menlo Park, CA.

Graizer, V., and A.F. Shakal (2004). “Analysis of CSMIP strong-motion geotechnical array recordings,” in P. de Alba, R.L. Nigbor, J.H. Steidl, and J.C. Stepp, editors, In Proceedings: *International Workshop for Site Selection, Installation, and Operation of Geotechnical Strong-Motion Arrays*, Richmond, CA, 2004. Consortium of Organizations for Strong Motion Observation Systems (COSMOS).

Graizer, V. (2014). “Comment on ‘Comparison of time series and random-vibration theory site-response methods’ by Albert R. Kottke and Ellen M. Rathje,” *Bull. Seismol. Soc. Am.*, **104,** 540–546.

Haddadi, H., A.F. Shakal, and C.R. Real (2008). “The Turkey Flat Blind Prediction Experiment for the September 28, 2004 Parkfield Earthquake: Comparison with Other Turkey Flat Recordings,” *Geotechnical Earthquake Engineering and Soil Dynamics IV Congress 2008*, pp. 1–10.

Haskell, N. (1960). “Crustal reflection of plane SH waves,” *J. Geophys. Res.* **65**, 4147–4450.

Kramer, S.L. (2009). “Analysis of Turkey Flat ground motion prediction experiment—Lessons learned and implication for practice,” *Proc. SMIP09 Seminar on Utilization of Strong-Motion Data*, Oakland, CA, pp.1–22.

Kwok, A.O.L., J.P. Stewart, and Y.M.A. Hashash (2008). “Nonlinear ground-response analysis of Turkey flat shallow stiff-soil site to strong ground motion,” *Bull. Seismol. Soc. Am.* **98**, 331–343.

Real, C.R. and B.E. Tucker (1988). “Ground Motion Site Effects Test Area Near Parkfield, California,” *Proceedings Ninth World Conference on Earthquake Engineering, Tokyo, Japan VIII*, pp. 187–191.

Real, C.R., A.F. Shakal, and B.E. Tucker (2006). “Turkey Flat, U.S.A. site effects test area: Anatomy of a blind ground-motion prediction test,” *Proceedings, 3rd International Symposium Effects of Surface Geology on Seismic Motion, 29 August–1 September 2006*, Grenoble, France, Paper KN 3, pp. 1–19.

Real, C., A. Shakal, and B. Tucker (2008). “The Turkey Flat Blind Prediction Experiment for the September 28, 2004 Earthquake: General Overview and Models Tested,” *Geotechnical Earthquake Engineering and Soil Dynamics IV Congress 2008*, pp. 1–10.

Tsai, C.-C., W.-S. Chang, and J.-S. Chiou (2017). “Enhancing Prediction of Ground Response at the Turkey Flat Geotechnical Array,” *Bull. Seismol. Soc. Am*. **107**, 2043–2054.

U.S. Code of Federal Regulations, “Reactor Site Criteria,” Part 100, Chapter I, Title 10, “Energy.”

U.S. Code of Federal Regulations, “Domestic Licensing of Production and Utilization Facilities Part 50, Chapter I, Title 10, “Energy”.

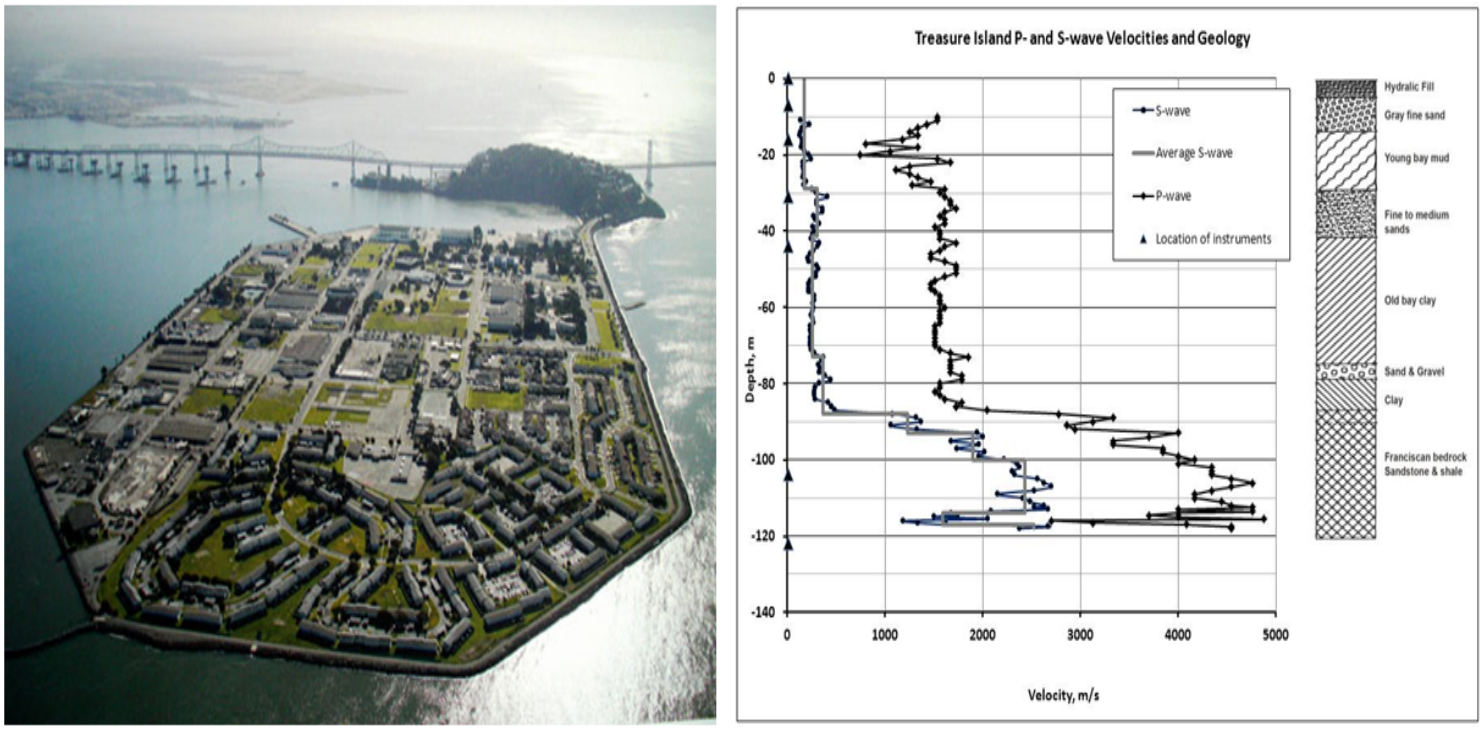

Figure 1. View of TI and YBI (left panel) and *P*- and *S*-wave velocities and soil profile at TI array (right panel). Triangles show locations of seismic instruments.

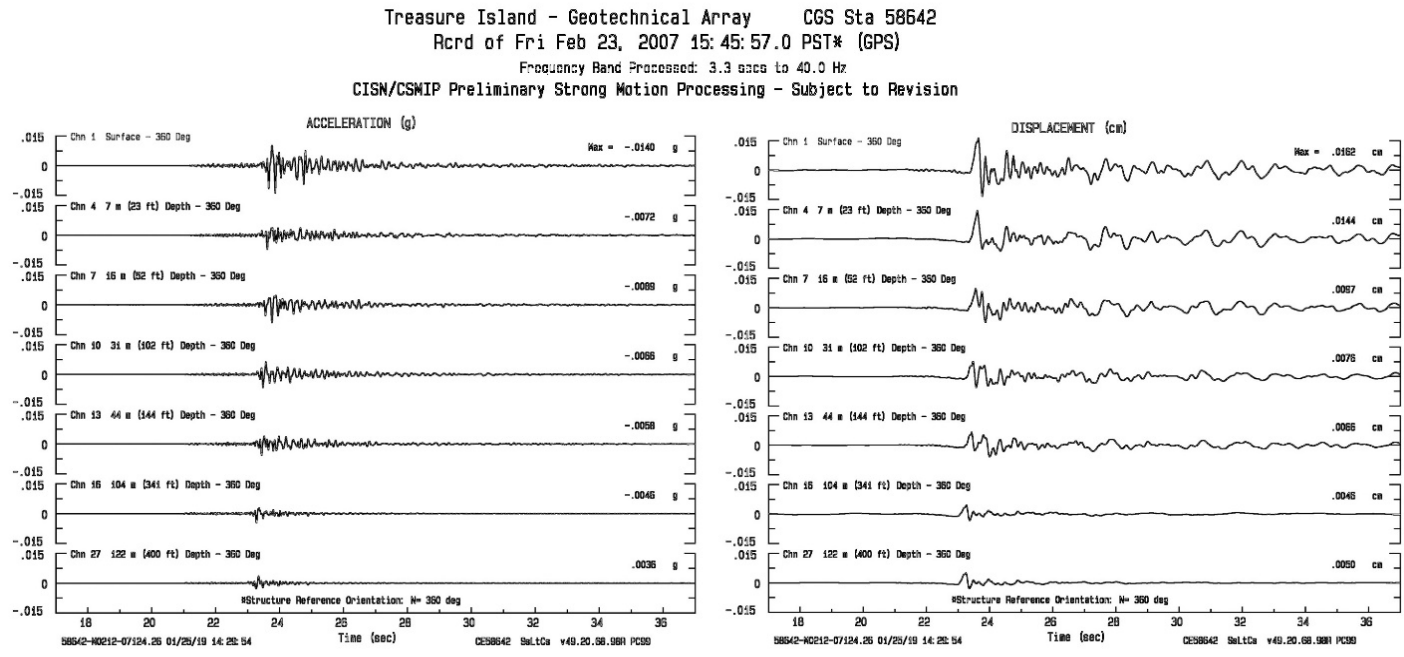

Figure 2. Shear waves dominated record of the M_L 3.4 earthquake with the epicenter at Berkeley, CA, at a distance of 12.5 km (Table 1): acceleration (left panel) and displacement (right panel).

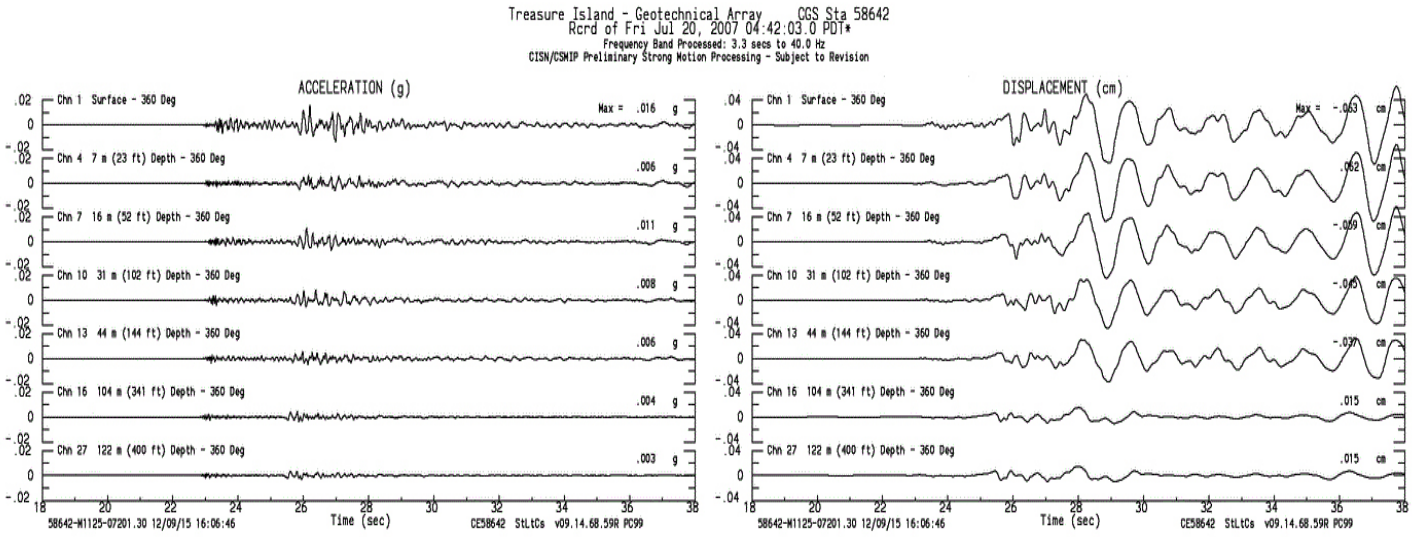

Figure 3. Surface waves dominated record of the M_W 4.2 earthquake with the epicenter at Piedmont, CA, at a distance of 16.5 km (Table 1): acceleration (left panel) and displacement (right panel).

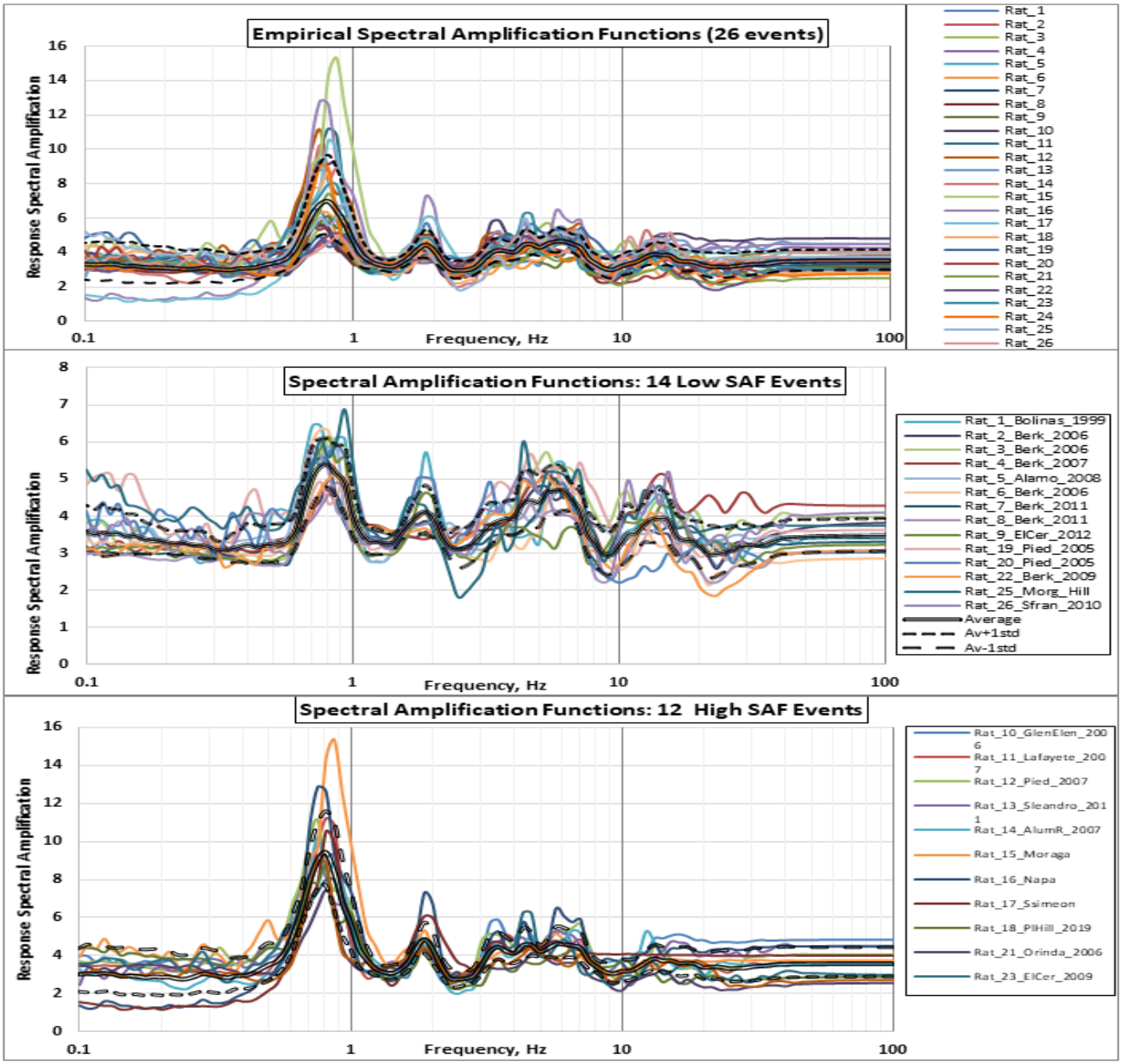

Figure 4. Response SAFs from bedrock at 122-m depth to the surface at the TI array: records from all 26 events (upper panel), records from 14 LAG events (middle panel), and records from 12 HAG events (lower panel).

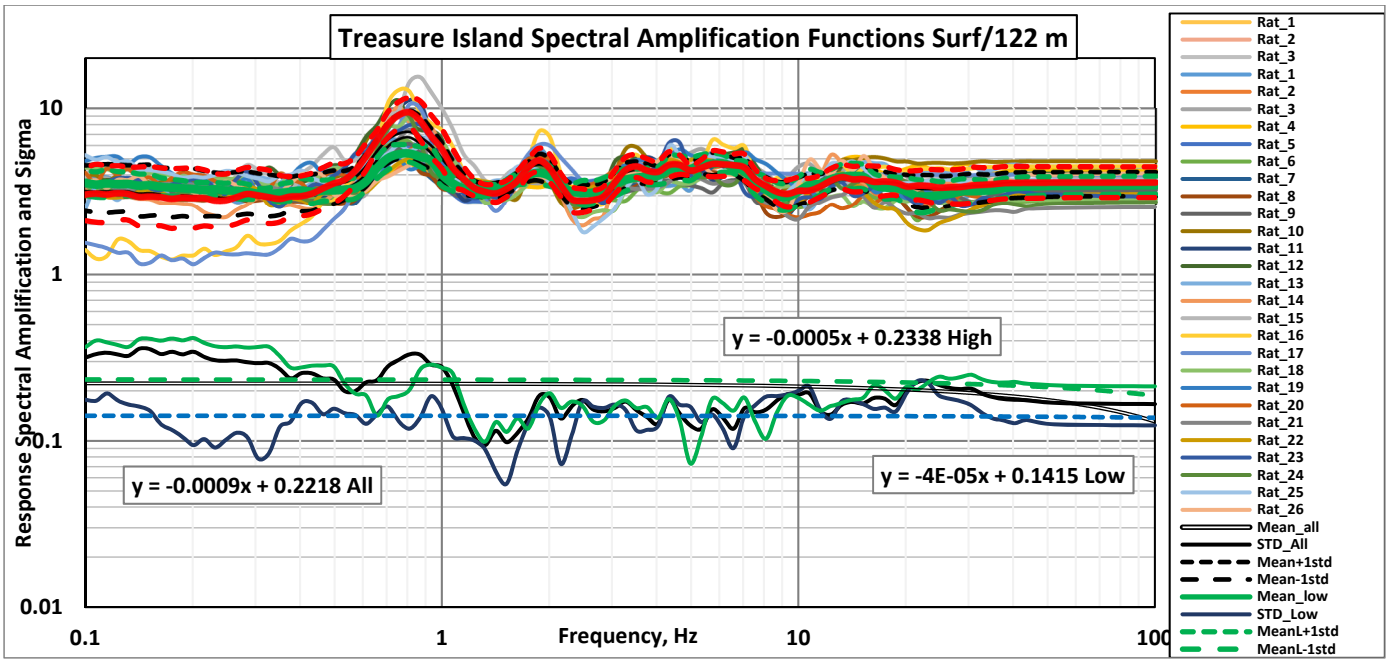

Figure 5. Response spectral SAFs and natural logarithmic standard deviations of SAFs for the TI downhole array surface/122-m depth.

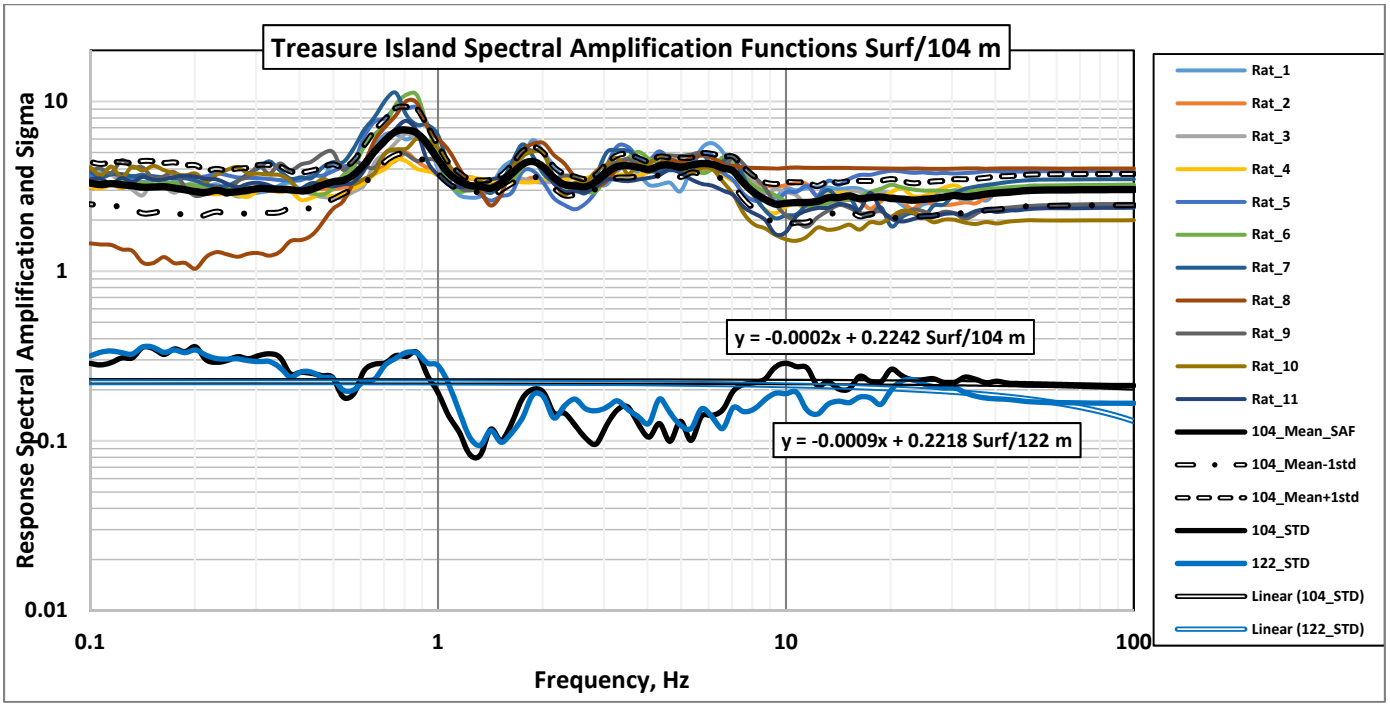

Figure 6. Response SAFs and natural logarithmic standard deviations of SAFs for the TI downhole array surface/104-m depth.

Figure 7. Map of TI and YBI stations. 58117 is the old TI Fire Station, and 58163 is the YBI Station. Those two stations recorded the 1989 M 6.9 Loma Prieta earthquake.

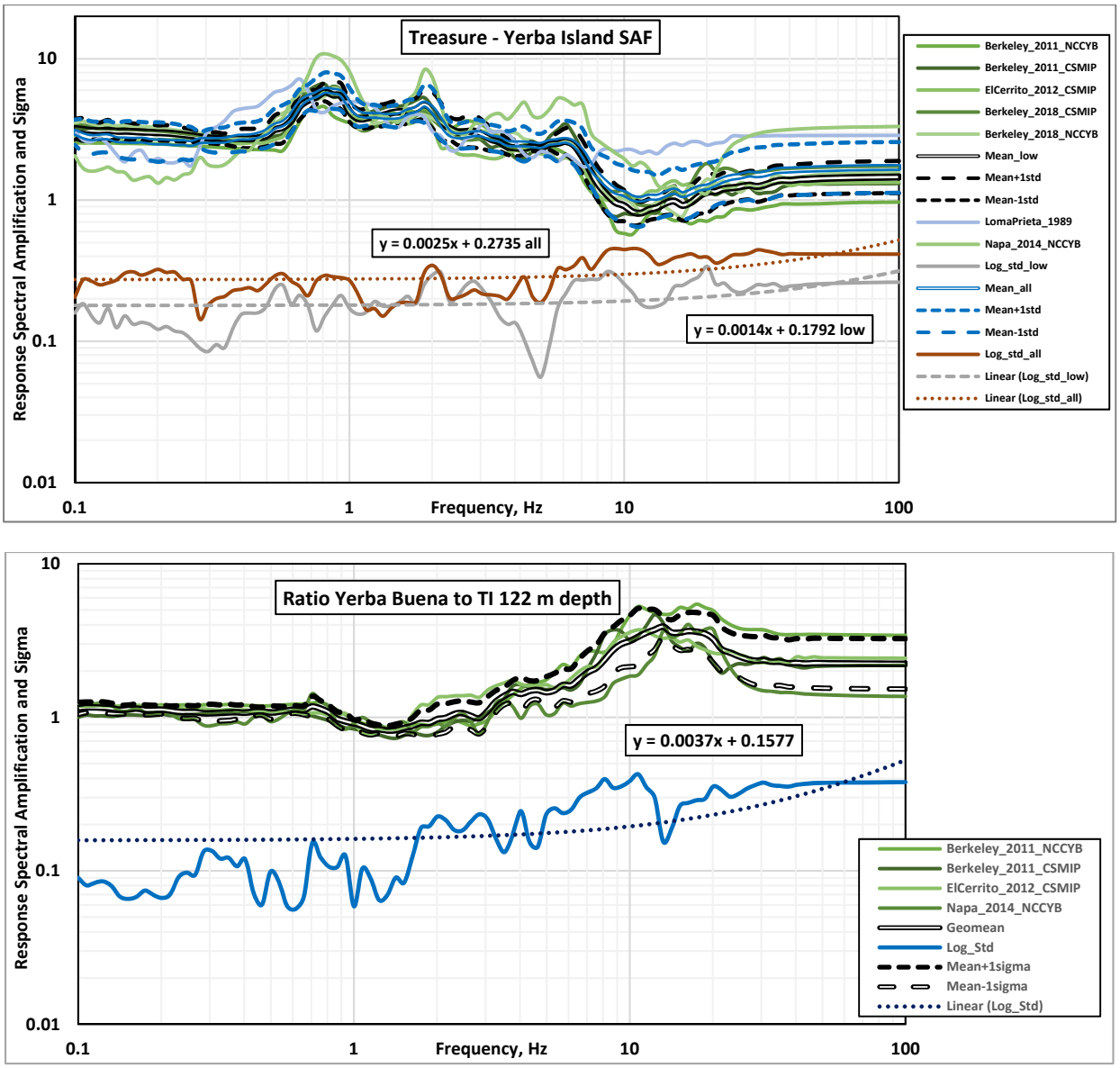

Figure 8. Response spectral SAFs and natural logarithmic standard deviations of SAFs for the TI surface to YBI (upper panel), and comparison of SAFs from the YBI to TI bedrock 122-m depth recordings (lower panel).

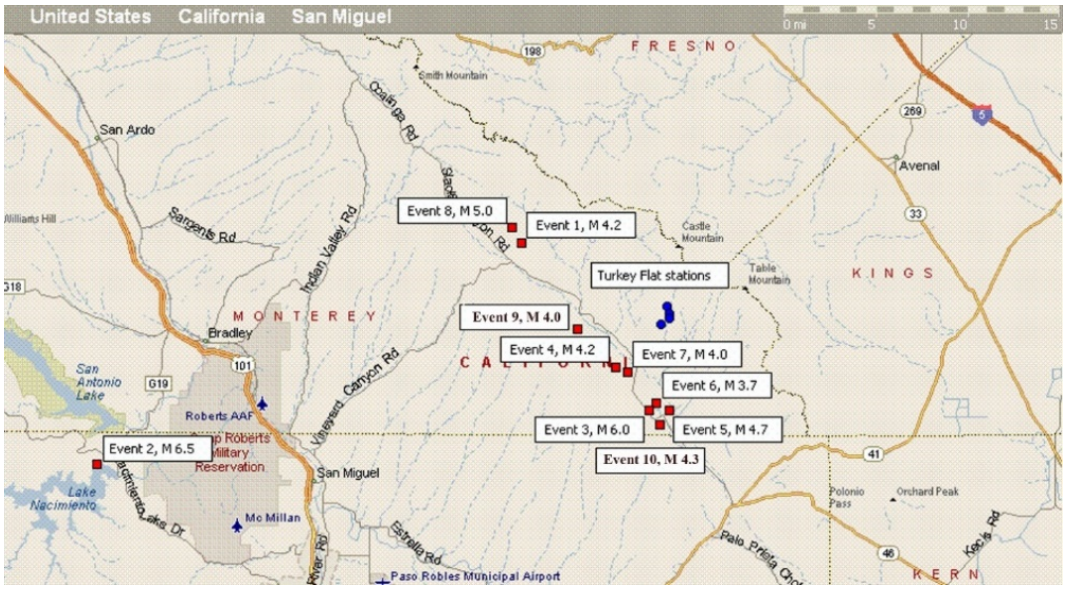

Figure 9. Map of earthquakes and Turkey Flat strong motion stations (modified from Haddadi et al., 2008).

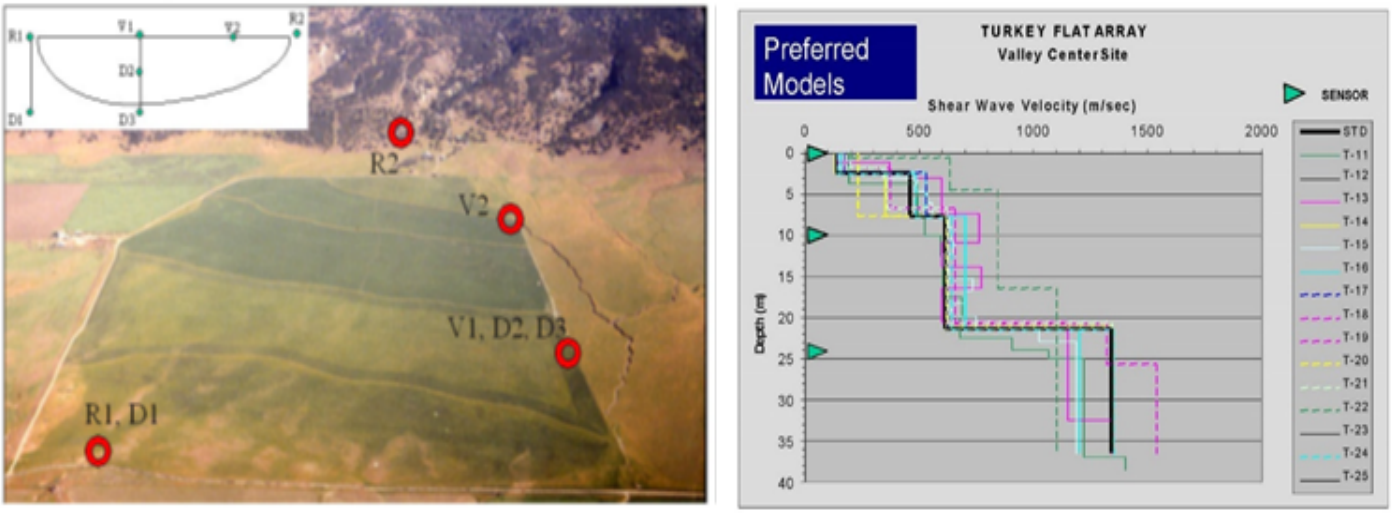

Figure 10. Oblique aerial view of Turkey Flat strong-motion array (Real et al., 2008) (left panel) and S-wave velocity profiles at mid-valley site (V1-D3 array) from Real et al., 2006 (right panel).

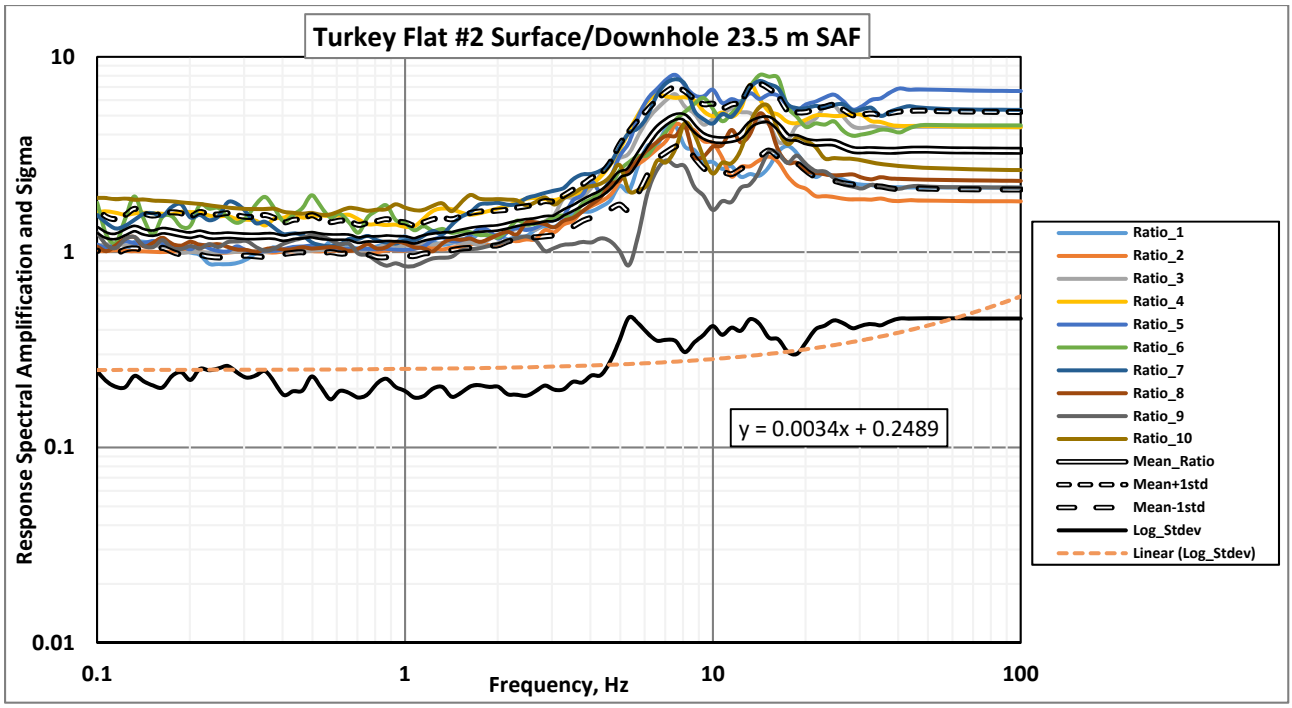

Figure 11. Response spectral SAFs and natural logarithmic standard deviations of SAFs for the Turkey Flat downhole array TF#2.

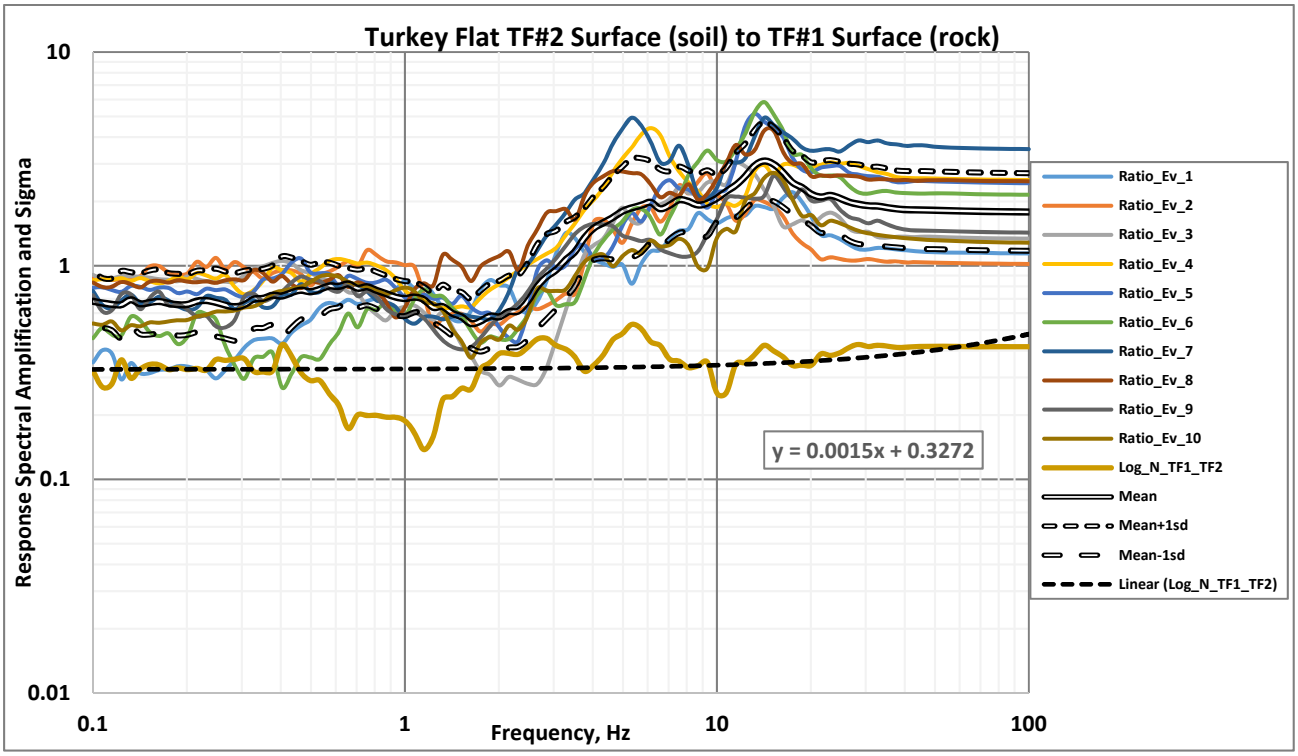

Figure 12. Response spectral SAFs and natural logarithmic standard deviations of SAFs for the Turkey Flat downhole array TF#2 surface to TF#1 surface.

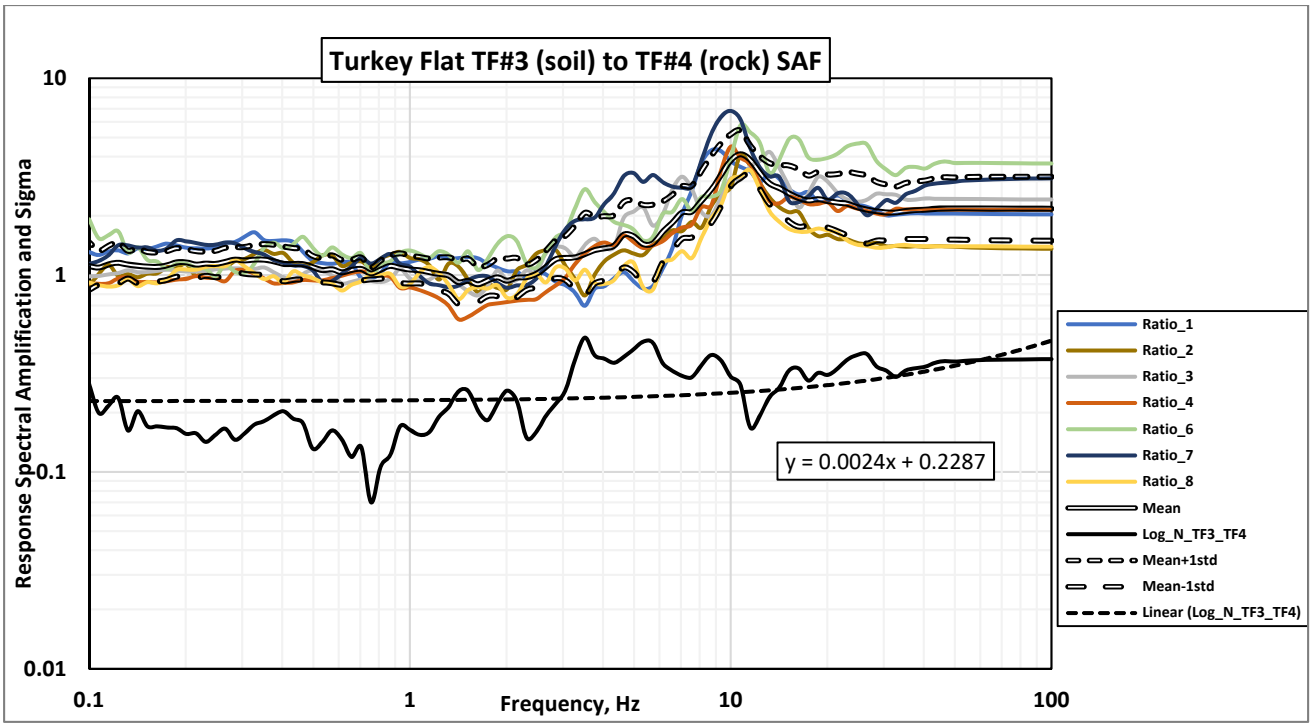

Figure 13. Response spectral SAFs and natural logarithmic standard deviations of SAFs for TF#3 (soil) to TF#4 (rock).

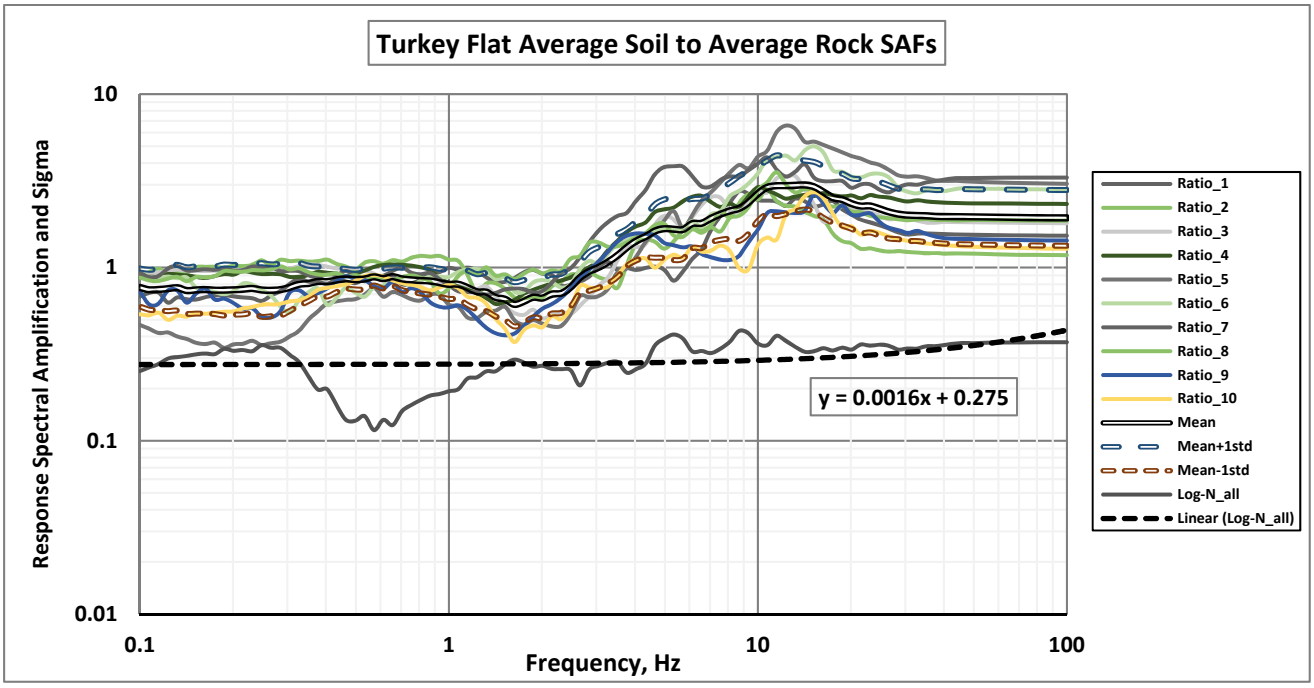

Figure 14. Response spectral SAFs and natural logarithmic standard deviations of SAFs for the Turkey Flat average soil/rock.

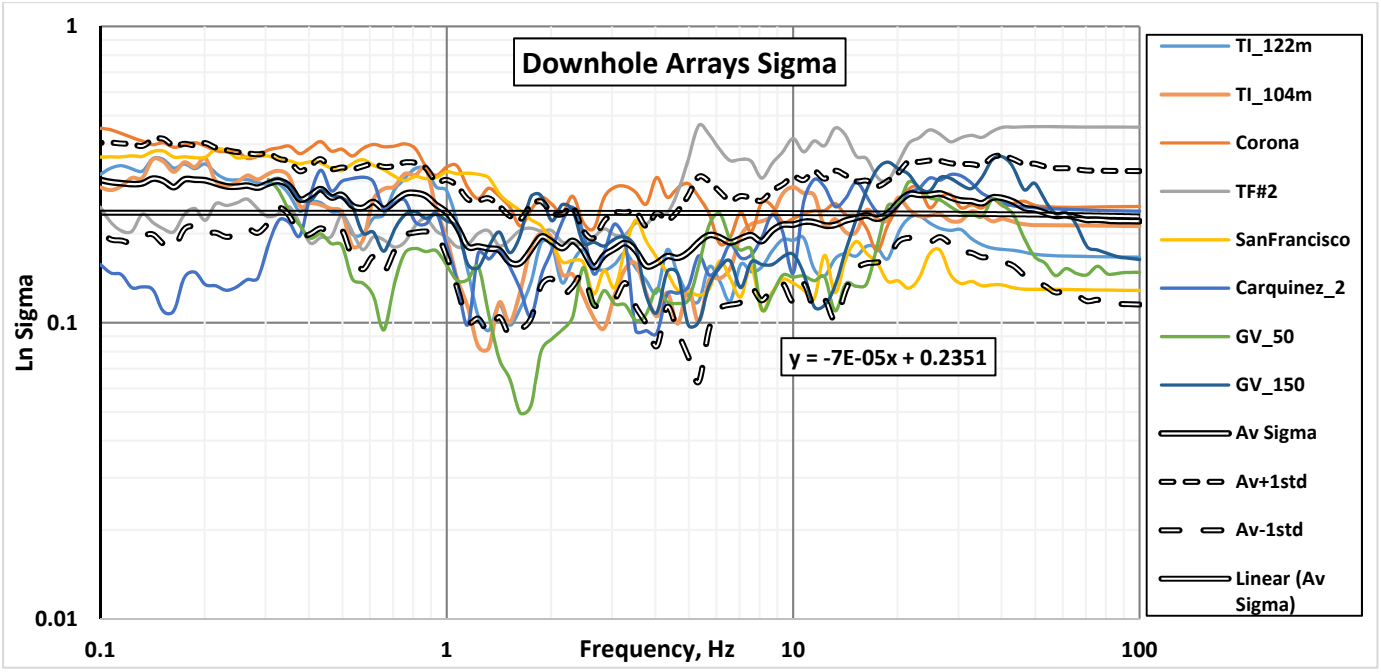

Figure 15. Frequency dependence of sigma σ_{ln} of the SAFs.

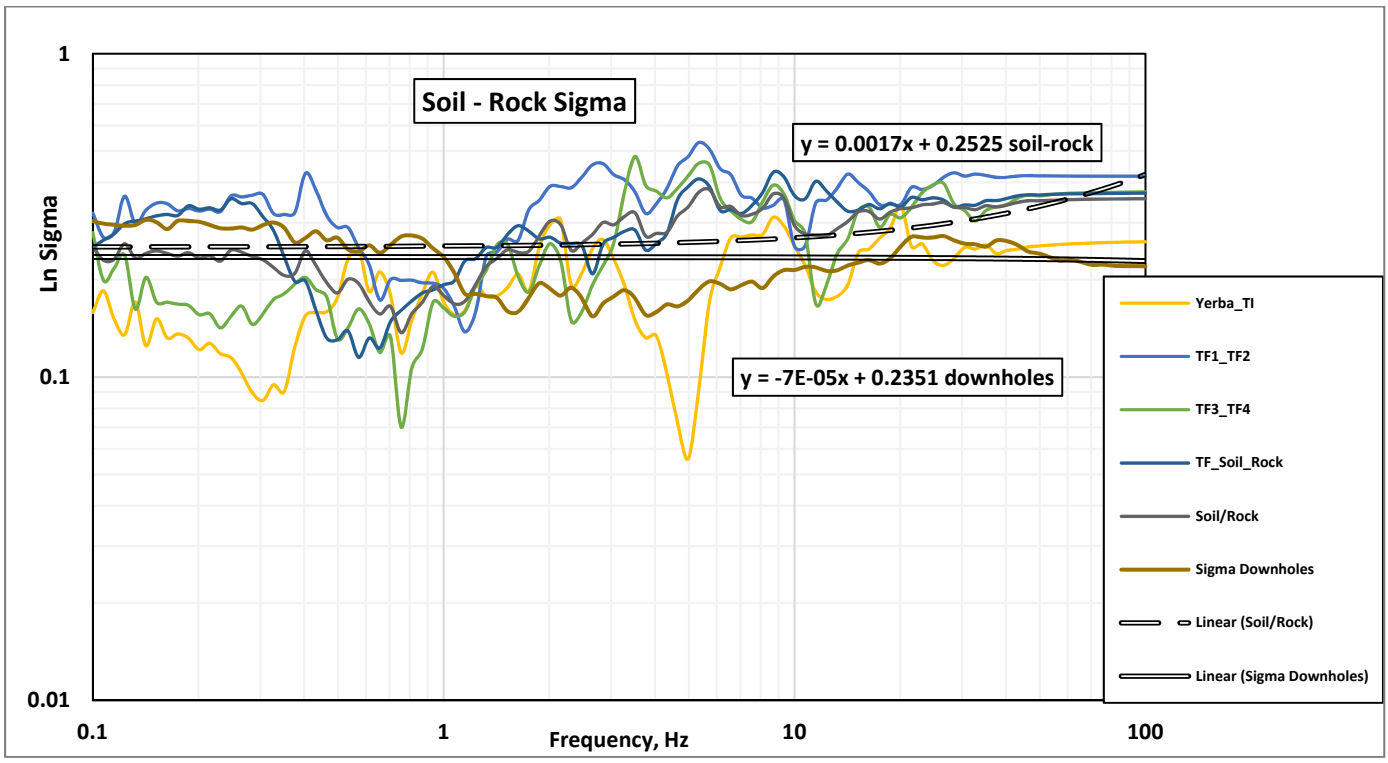

Figure 16. Soil-rock station pairs sigma compared to downhole arrays sigma.

APPENDIX A

ADDITIONAL DOWNHOLE ARRAYS SCHEMATIC SENSOR LOCATIONS AND *P*- AND *S*-WAVES VELOCITY PROFILES

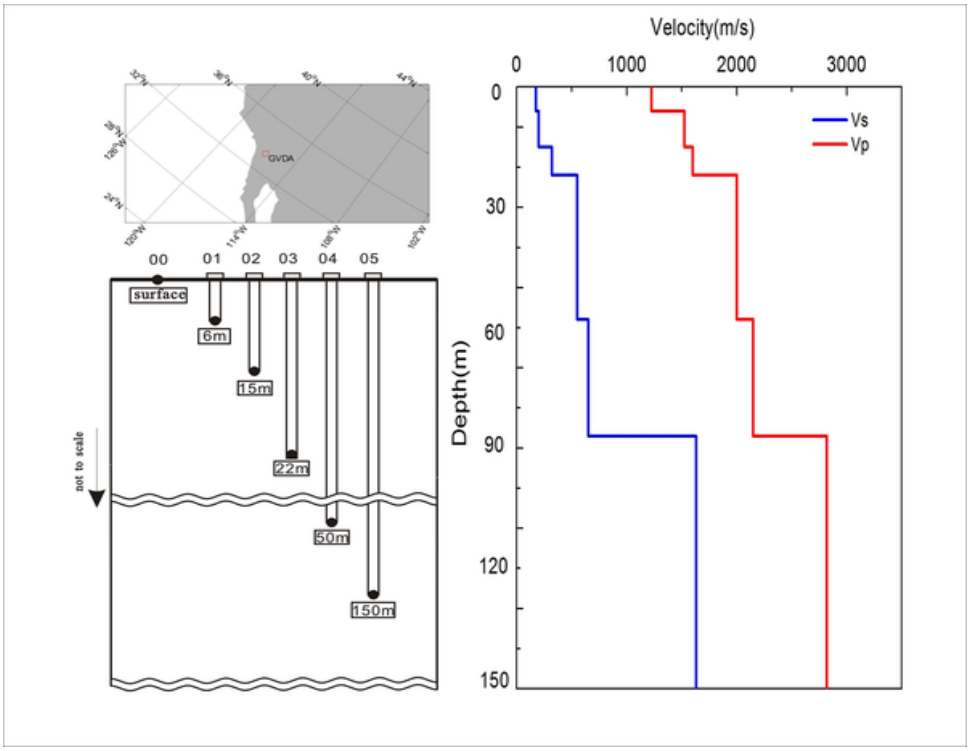

Figure A-1. Garner Valley downhole array (GVDA) and *P*- and *S*-wave velocity profiles. Downloaded from http://nees.ucsb.edu/facilities/GVDA.

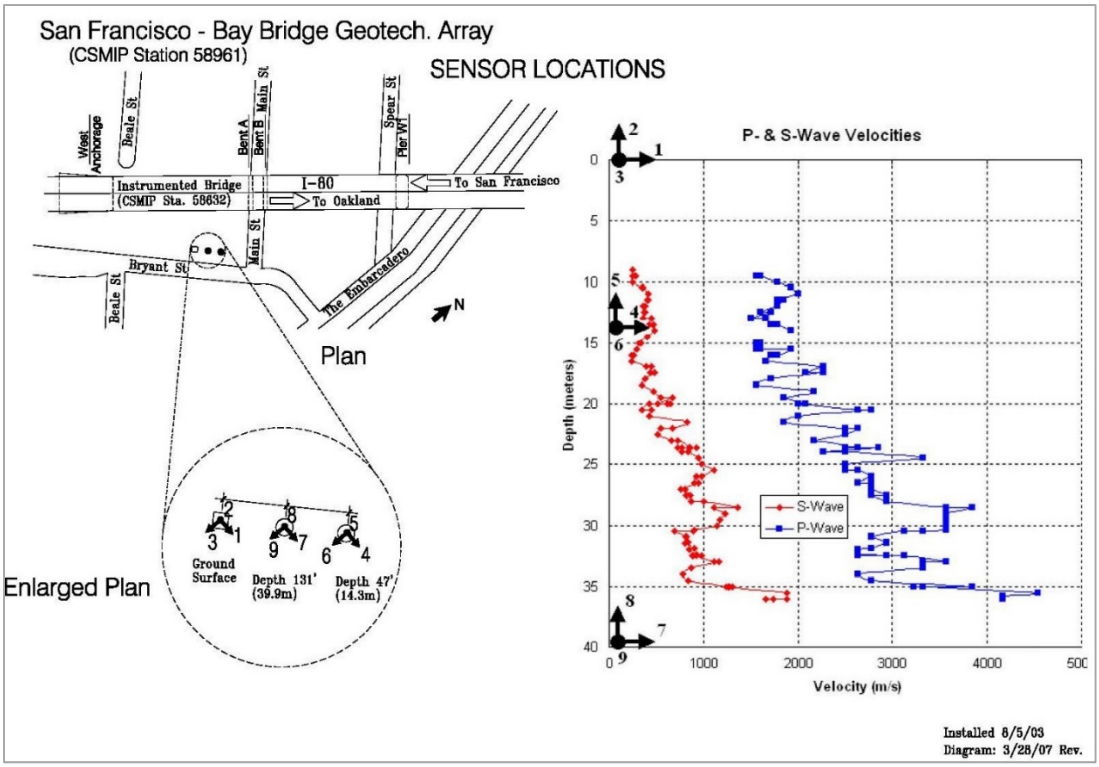

Figure A-2. San Francisco Bay Bridge Geotech Array (58961). Sensors: Surface,14.3, 39.9 meters (m). Downloaded from the Center for Engineering Strong Motion Data (CESMD) at https://strongmotioncenter.org/.

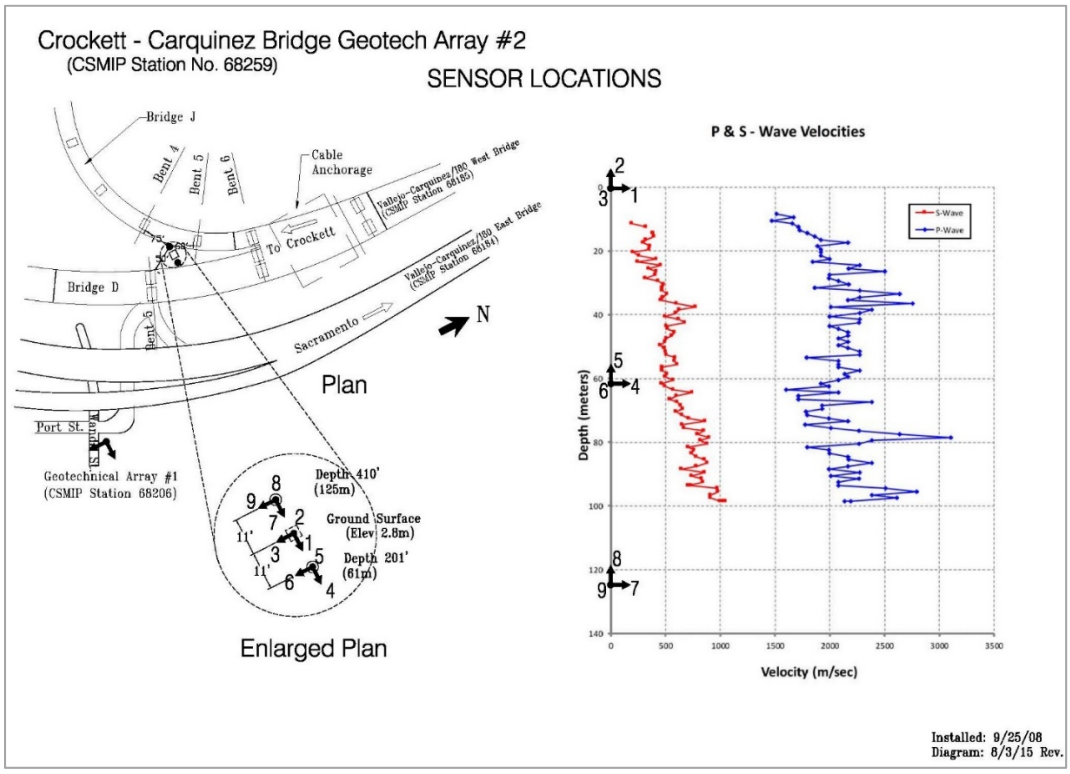

Figure A-3. Crockett Carquinez Bridge Geotech Array #2 (68259). Sensors: Surface, 61, 125 m. Downloaded from the CESMD at https://strongmotioncenter.org/.

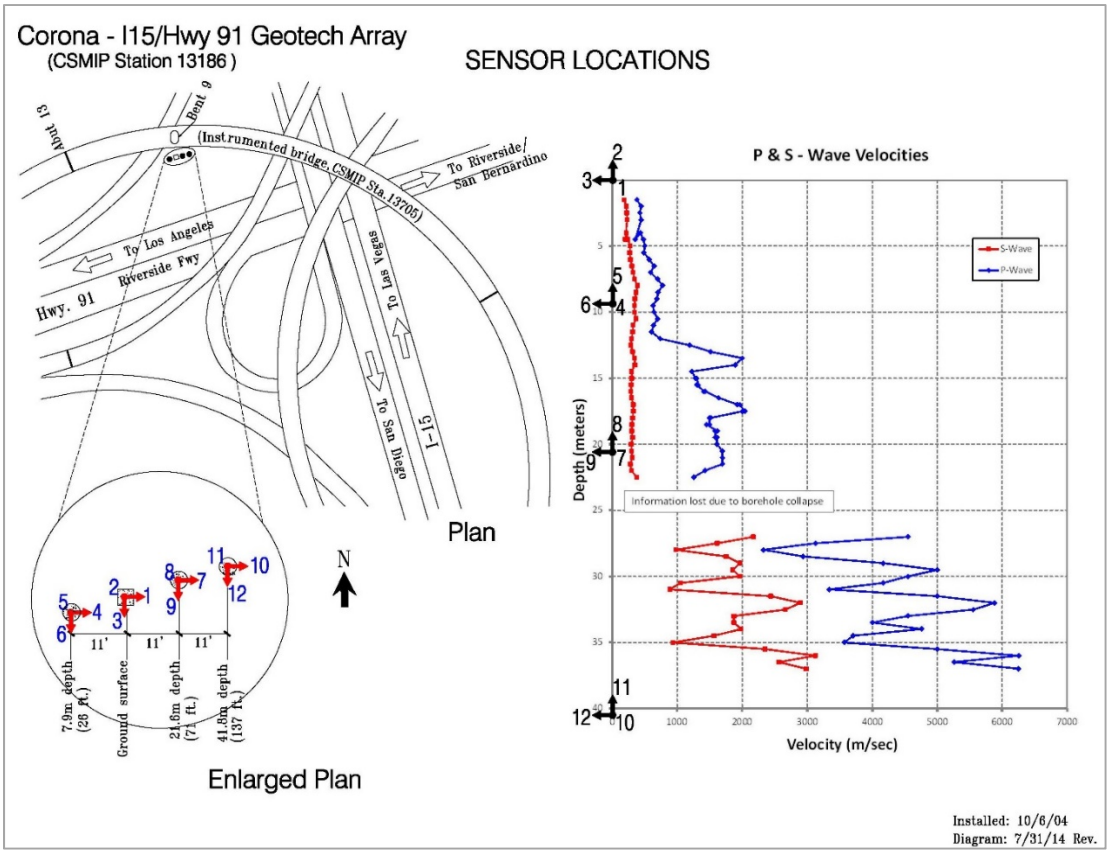

Figure A-4. Corona–I15/Hwy 91 Geotech Array (13186). Sensors: Surface, 7.9, 21.6, 41.8 m. Downloaded from the CESMD at https://strongmotioncenter.org/.

Table 1. Earthquakes recorded at the Treasure Island geotechnical array at the surface and at 122-m depth

Earthquake Name	Date	Time	Magnitude	Depth, km	Epicenter Dist., km	Surface PGA
S-waves dominated lower amplification group						
Bolinas	1999-08-17	18:06:18 PDT	5.0 M_L	6.9	29.0	0.018
Piedmont	2005-05-08	3:35:55 PDT	3.3 M_W	5.0	13.1	0.003
Piedmont	2005-09-24	4:25:16 PDT	3.3 M_W	5.4	13.5	0.002
Berkeley	2006-12-22	22:49:57 PST	3.6 M_L	9.2	11.9	0.029
Berkeley	2006-12-23	09:21:15 PST	3.4 M_L	9.3	11.6	0.015
Berkeley	2007-02-23	15:46:15 PST	3.4 M_L	10.9	12.5	0.019
Alamo	2008-09-05	21:00:15 PDT	4.0 M_W	16.2	33.6	0.025
Berkeley	2009-05-13	15:34:05 PDT	3.1 M_W	10.8	13.2	0.004
San Francisco	2010-06-28	07:47:04 PDT	3.3 M_W	7.7	18.6	0.003
Morgan Hill	2011-01-07	16:10:16 PST	4.1 M_L	7.1	86.5	0.005
Berkeley	2011-10-20	14:41:04 PDT	4.0 M_W	8.0	11.7	0.023
Berkeley	2011-10-20	20:16:05 PDT	3.8 M_W	9.6	11.8	0.038
Berkeley	2011-10-27	05:36:44 PDT	3.6 M_L	9.7	12.1	0.013
El Cerrito	2012-03-05	05:33:19 PST	4.0 M_L	9.2	13.1	0.019
Surface waves dominated higher amplification group						
San Simeon	2003-12-22	11:15:56 AM PST	6.5 M_W	4.7	261.0	0.004
Orinda	2006-03-01	11:34:52 PST	3.4 M_W	8.3	14.9	0.006
Glen Ellen	2006-08-02	20:08:12 PDT	4.4 M_L	9.1	52.1	0.014
Lafayette	2007-03-01	20:40:00 PST	4.2 M_L	16.6	25.7	0.014
Berkeley	2011-07-16	03:31:26 PDT	3.3 M_W	6.0	11.0	0.004
Piedmont	2007-07-20	04:42:22 PDT	4.2 M_W	5.8	16.5	0.018
San Leandro	2011-08-23	23:36:54 PDT	3.6 M_L	8.1	21.8	0.007
Alum Rock	2007-10-30	20:04:54 PDT	5.4 M_W	9.2	68.5	0.012
Moraga	2008-06-06	02:02:53 PDT	3.5 M_W	7.6	26.3	0.003
El Cerrito	2009-06-06	15:30:56 PDT	3.3 M_W	5.6	12.0	0.003
South Napa	2014-08-24	03:20:44 PDT	6.0 M_W	11.3	44.1	0.017
Pleasant Hill	2019-10-14	22:33:42 PDT	4.5 M_W	14.0	30.5	0.011

Table 2. Earthquakes recorded at Yerba Buena and surface channels of Treasure Island

Earthquake Name	Date	Time	Magnitude	Depth, km	Epicenter Dist., km	Surface PGA	Epicenter Dist., km	PGA
					Treasure Island		Yerba Buena	
Loma Prieta	1989-10-17	17:04:00 PDT	6.9 M_W	18.0	97.7	0.160	95.4	0.060
Berkeley	2011-10-20	14:41:04 PDT	4.0 M_W	8.0	11.7	0.023	11.7	0.021
Berkeley	2011-10-20	20:16:05 PDT	3.8 M_W	9.6	11.8	0.038	11.8	0.039
El Cerrito	2012-03-05	05:33:19 PST	4.0 M_L	9.2	13.1	0.019	14.5	0.015
South Napa	2014-08-24	03:20:44 PDT	6.0 M_W	11.3	44.1	0.017	45.9	0.005
Berkeley	2018-01-04	02:39:37 PDT	4.4 M_W	12.3	10.8	0.064	10.7	0.042
Pleasant Hill	2019-10-14	22:33:42 PDT	4.5 M_W	14.0	30.5	0.011	30.5	0.005

Table 3. Events producing moderate to strong motions at Turkey Flat array (updated after Haddadi et al., 2008)

Event No.	Event Name	Date	Time	Mag	Epicenter Lat	Epicenter Lon	Distance from Epicenter to: TF#1	TF#2	TF#3	TF#4	PGA @ Surface TF#1	TF#2	TF#3	TF#4
1	Parkfield	4/3/1993	21:21:24 PST	4.2	35.942	120.493	14.1	14.5	14.3	13.9	0.026	0.033	0.081	0.047
2	**San Simeon**	12/22/2003	11:15:56 PST	6.5	35.710	121.100	69.6	70.4	70.6	70.6	0.035	0.036	0.031	0.023
3	**Parkfield (Mainshock)**	9/28/2004	10:15:24 PDT	6.0	35.810	120.370	7.6	8.2	8.6	9.2	0.245	0.300	0.260	0.110
4	Aftershock	9/28/2004	10:19:24 PDT	4.2	35.844	120.402	5.5	6.3	6.6	7.0	0.052	0.170	0.072	0.034
5	Aftershock	9/28/2004	10:24:15 PDT	4.7	35.810	120.350	7.6	8.0	8.4	9.1	0.046	0.074	0.053	0.013
6	Aftershock	9/28/2004	10:33:56 PDT	3.7	35.815	120.363	7.0	7.5	8.0	8.6	0.016	0.026	0.026	0.006
7	Aftershock	9/28/2004	12:31:27 PDT	4.0	35.840	120.390	5.1	5.9	6.3	6.7	0.012	0.049	0.024	0.008
8	Aftershock	9/29/2004	10:10:04 PDT	5.0	35.954	120.502	15.5	15.9	15.7	15.2	0.016	0.042	0.037	0.030
9	Parkfield	5/22/2007	04:34:12 PDT	4.0	35.860	120.414	5.4	6.3	NR*	NR	0.035	0.054	NR	NR
10	Cholame	12/17/2019	10:29:21 PST	4.3	35.806	120.356	7.9	8.5	NR	NR	0.051	0.047	NR	NR

Table 4. Average logarithmic standard deviation

Site	Average in range of 0.3–40 Hz	
	Log_Nat_Sigma σ_{ln}	Ratio
Treasure Island 122 m	0.189	*1.208*
Treasure Island 104 m	0.202	*1.224*
Corona Bridge	0.282	*1.326*
TF#2	0.287	*1.332*
San Francisco Bay Bridge	0.211	*1.235*
Crockett Carquinez_2	0.216	*1.241*
Garner Valley 50 m	0.163	*1.177*
Garner Valley 150 m	0.218	*1.243*
Av Sigma	***0.221***	***1.247***
Yerba_TI	0.203	*1.225*
TF1_TF2	0.341	*1.407*
TF3_TF4	0.263	*1.301*
TF_Soil_Rock	0.282	*1.326*
Av Sigma	***0.272***	***1.313***